Petroleum Science 20 (2023) 1119–1128

Contents lists available at ScienceDirect

Petroleum Science

journal homepage: www.keaipublishing.com/en/journals/petroleum-science

Original Paper

Degradation of chemical and mechanical properties of cements with different formulations in CO_2-containing HTHP downhole environment

Wei Yan [a, *], Hao-Guang Wei [b], Nguu Dickson Muchiri [a], Fu-Li Li [a], Jing-Ru Zhang [a], Zheng-Xian Xu [a]

[a] State Key Laboratory of Petroleum Resources and Prospecting, China University of Petroleum, Beijing, 102249, China
[b] Sinopec Petroleum Engineering Technology Research Institute Co., Ltd., Beijing, 102206, China

ARTICLE INFO

Article history:
Received 28 December 2022
Received in revised form
25 February 2023
Accepted 16 March 2023
Available online 17 March 2023

Edited by Jia-Jia Fei

Keywords:
HPHT reservoirs
Oil well cement
CO_2 corrosion
Chemo-mechanical
Mechanical properties
Micro-indentation

ABSTRACT

The increasing energy demand has pushed oil and gas exploration and development limits to extremely challenging and harsher HTHP (High Temperature and High Pressure) environments. Maintaining wellbore integrity in these environments, particularly in HPHT reservoirs with corrosive gases, presents a significant challenge. Robust risk evaluation and mitigation strategies are required to address these reservoirs' safety, economic, and environmental uncertainties. This study investigates chemo-mechanical properties degradations of class G oil well cement blended with silica fume, liquid silica, and latex when exposed to high temperature (150 °C) and high partial pressure of CO_2 saturated brine. The result shows that these admixtures surround the cement grains and fill the interstitial spaces between the cement particles to form a dense crystal system of C–S–H. Consequently, the cement's percentage of pore voids, permeability, and the content of alkali compounds reduce, resulting in increased resistance to CO_2 corrosion. Liquid silica, a specially prepared silica suspension, is a more effective alternative to silica fume in protecting oil well cement against CO_2 chemical degradation. Micro-indentation analysis shows a significant deterioration in the mechanical properties of the cement, including average elastic modulus and hardness, particularly in the outer zones in direct contact with corrosive fluids. This study highlights the significance of incorporating admixtures to mitigate the effects of CO_2 corrosion in HPHT environments and provides a valuable technique for quantitatively evaluating the mechanical-chemical degradation of cement sheath.

1. Introduction

The global energy demand continues to grow, driving the energy sector to explore increasingly challenging environments. With most easily accessible resources depleted, attention has turned to previously classified inaccessible oil and gas resources, including deep offshore and ultra-deep high-pressure, high-temperature (HPHT) reservoirs. These resources present inherent challenges, and their successful and cost-effective development depends on well design and construction. Maintaining zonal isolation and safeguarding well-completion systems is essential to prevent process safety breaches. However, maintaining the integrity of wells drilled in sour gas HPHT reservoirs is challenging due to corrosive gases, particularly H_2S and CO_2 (Carpenter, 2022; Wei et al., 2015; Li et al., 2016; Kiran et al., 2017). When cement is exposed to CO_2 saturated-brine environment, a series of physico-chemical reactions occur (Carroll et al., 2016), as shown in Eqs. (1)–(5) (Duguid and Scherer, 2010; Gu et al., 2017; Kutchko et al., 2007).

Initially, CO_2 dissolves in water, producing unstable carbonic acid, further dissociating and releasing carbonate ions (CO_3^{2-}) and hydrogen H^+. The cement's portlandite (CH) phase is assumed to react first, producing a sparingly soluble calcium carbonate precipitate. As the reaction proceeds, a thin layer of carbonate may be formed on the surface of portlandite and subsequently limit any further reactions. However, the depletion of portlandite phases on

* Corresponding author.
E-mail address: yanwei@cup.edu.cn (W. Yan).

https://doi.org/10.1016/j.petsci.2023.03.012

the cement matrix gradually decreases the solution's pH, and thus bicarbonate ions become the dominant species. As a result, the dissolution of calcium on the abundant cement hydration products (silicate phases) takes effects leaving behind $SiO_{2(amorphous)}$ (amorphous silica gel).

$$CO_{2(g)} + H_2O \leftrightarrow H_2CO_{3(aq)} \leftrightarrow H^+_{(aq)} + HCO^-_{3(aq)} \leftrightarrow 2H^+_{(aq)} + CO^{2-}_{3(aq)} \quad (1)$$

$$Ca(OH)_{2(s)} + 2H^+_{(aq)} + CO^{2-}_{3(aq)} \leftrightarrow CaCO_{3(s)} + 2H_2O \quad (2)$$

$$CSH_{(s)} + 2H^+_{(aq)} + CO^{2-}_3(aq) \leftrightarrow CaCO_{3(s)} + H_2O + SiO_{2(amorphous)} \quad (3)$$

$$CaCO_{3(s)} + CO_{2(aq)} + H_2O \leftrightarrow Ca^{2+}_{aq} + 2HCO^-_{3(aq)} \quad (4)$$

$$H^+_{aq} + CaCO_{3(aq)} \leftrightarrow Ca^{2+}_{aq} + HCO^-_{3(aq)} \quad (5)$$

Due to carbonation, cement sheath microstructural properties, including porosity, transport properties, and mechanical strength, are altered (Kutchko et al., 2009; Zhang et al., 2020a, b). In recent years, research has been conducted to investigate the effect of carbonation on cement's mechanical properties and to develop new cement systems that can withstand carbonation. Todorovic et al. (2020) investigated the mechanical properties of a novel cement system with an expandable agent in carbonated brine. The results showed that the mechanical properties of the cement system were significantly affected by long-term aging in carbonated brine. Chavez Panduro et al. (2020) studied the carbonation of Portland cement in real-time 3D observations at CO_2 storage conditions. The study employed X-ray microtomography to visualize and quantify the carbonation process in cement samples. The results showed that the carbonation of cement was heterogeneous, with the process starting from the surface and progressing inward. The carbonation process resulted in the formation of calcium carbonate crystals, reducing the pore size and increasing the cement density. Carbonation depth has generally been adopted as a key indicator for predicting the long-term integrity of cement-based materials. Spraying phenolphthalein indicator has been the conventional method to determine carbonation depth (Chang and Chen, 2006). However, studies have challenged this concept by demonstrating that a partially carbonated zone occurs where pH is problematic to detect using a phenolphthalein indicator (Parrott, 1987).

Various models have been developed to predict the extent of carbonation of cement sheaths in oil and gas wells. Several of these models use a diffusion-controlled mechanism to describe the transport of CO_2 in the cement (Huet et al., 2010). With the current growth in computing power, more complex numerical modeling of cement degradation can be performed to provide comprehensive and accurate mathematical models for predicting oil well cement integrity. Gherardi et al. (2012) utilized numerical simulations to predict the evolution of fluid chemistry and mineral alteration in the cement of an idealized abandoned wellbore in the Paris Basin, France, where CO_2 geological disposal is under consideration. The simulations revealed that the interaction of cement with acid fluids from the reservoir caused severe mineralogical alteration of the cement, resulting in a two-stage evolution of the porous cement matrix. The first stage, termed the "clogging" stage, was characterized by decreased porosity due to calcite precipitation. The second stage was a reopening of porosity related to the disappearance of primary cement phases and the re-dissolution of secondary minerals such as zeolites.

This study comprehensively investigates the changes in material properties of various cement formulations when exposed to CO_2-saturated brine. The analysis is conducted through micro-indentation and visual examination techniques to gain a deeper understanding of the behavior of cement formulations in CO_2-corrosive gas environments. One of the primary applications of this research is in enhancing wellbore integrity. Cement sheath failure can lead to sustained casing pressure, which poses a significant risk to wellbore integrity. Understanding the mechanical properties of different cement formulations under CO_2-corrosive gas conditions is crucial.

Micro-indentation analysis is used to determine the mechanical properties of the samples before and after carbonation at different zones. This technique allows for the accurate characterization of changes in mechanical properties such as hardness and elastic modulus (Woirgard et al., 1998; Constantinides et al., 2003; Han et al., 2012a; Zhang et al., 2020a, b). X-ray diffraction analysis (XRD), SEM analysis, and phenolphthalein tests are conducted to examine the degree of carbonation and identify any mineralogical changes that may occur. The findings of this study have significant implications for enhancing wellbore integrity and preventing casing pressure buildup and can provide valuable insights into the behavior of cement systems in HPHT corrosive gas reservoirs.

2. Materials and methods

2.1. Preparation of samples

Three batches of cement slurry were prepared separately by mixing class G cement with water and other additives, as shown in Table 1. The API (API 10B-2013) guideline defines class G slurry as 100 parts of dry cement by weight to 44 parts of mixing water by weight. Cement and water were added to the mixing devices according to the ratios stipulated in the API guideline. After attaining the required slurry consistency, we poured the mixture into cubes measuring 50 mm × 50 mm × 50 mm, which were then machined and cored after curing to create ø 25 mm by 50 mm in length core samples.

2.2. CO_2 - saturated brine chemical degradation test

Core samples from each batch group were placed in a high-temperature-high-pressure autoclave containing 2000 mL of synthetic brine to simulate the reservoir brine composition. Then, nitrogen was injected into the vessel for 2 h to deoxidize. Subsequently, the temperature was raised to 150 °C, and the brine was saturated with CO_2 at a pressure of 4 MPa. The test parameters are sourced from the actual downhole condition of a southwest oil field in China, a typically high-temperature, high-pressure (HTHP) well (Shadravan and Amani, 2012; Phi et al., 2019). The CO_2 reaction was then allowed to take place for four weeks. The pressure was maintained at 4 MPa throughout the reaction period. The freshly reacted core sample surfaces were then sprayed with phenolphthalein indicator.

Table 1
Composition of different cement formulations.

Mix No.	Types of Additives	wt%
15 (Base Mix)	Silica fume	40
	Fluid-loss additive	6
	Retarder	0.5
16 (Base Mix + Other additives)	Liquid silicon	10
20 (Base Mix + Other additives)	Latex	16

2.3. Porosity and permeability test

The experiment involved measuring the permeability and porosity of cement samples before being subjected to chemical degradation. Porosity was measured using a Helium porosimeter (KXD-III), which takes advantage of the molecular size of Helium to enter rapidly the micropore system. The core sample was placed in a holder, the pressure was applied, and Helium from a reference chamber expanded into the pore volume. Equilibrium pressure was measured, and pore volume was estimated. Permeability was measured using the transient pressure pulse method (PDP-200) before and after the reaction with CO_2. This method involved applying a confining pressure load and generating a pressure pulse to allow gas to flow across the sample. The computer system continuously monitored real-time pressure changes and calculated sample permeability based on upstream and downstream pressure attenuation curves. The fully automated system enables automatic control, data acquisition, processing, and test report generation.

Next, the carbonation process was initiated, and the specimens were allowed to react with CO_2 for a specific time. Following the completion of the reaction, the samples underwent a drying process at 65 °C for 32 h to eliminate any surplus moisture and guarantee complete dryness before evaluating their porosity and permeability. Subsequently, the samples were subjected to the same pressure gradient to calculate their permeability, and the porosity was again determined using the same methodology as before. By comparing the porosity and permeability obtained before and after the reaction, the change in the microstructure of the cement samples resulting from the carbonation reaction was evaluated quantitatively.

2.4. Uniaxial compressive strength test

The compression strength of the samples was determined using a TAW-1000 computerized electrohydraulic servo pressure loading system with a maximum load capacity of 1000 kN. The system consists of several components, including a load cell that measures the force applied to the sample, a hydraulic pump system that applies the load, a central control unit that regulates the system, and a couple of sensors that monitor the sample's deformation during loading. Before testing, the samples were placed inside a polyethylene sleeve to protect them from external influences, and gauges were carefully attached to measure circumferential and axial deformations during loading. After preparation, the sample was placed on the apparatus, and the linear vertical displacement transducer was adjusted to align the load cell piston with the sample. Loading then commenced at a 0.2 mm/min rate until the specimen failed. Once the sample failed, the loading was manually stopped, and the test data was saved for further analysis. The procedure was repeated for samples before and after CO_2 corrosion to compare the compression strength results.

2.5. Microstructural analysis

2.5.1. Indentation test

Small pieces of cement obtained after the CO_2 reaction were immersed in an isopropanol solution for 24 h to stop further CO_2 reactions. Then they were dried and embedded in epoxy resin in 3 cm diameter holders (Fig. 1). The sample surfaces were manually polished with medium, fine, ultra-fine SiC grade sandpapers to decrease their surface roughness. After polishing, the surfaces were cleaned off the polishing suspension and other particles.

The micromechanical properties of the dressed samples were then studied by UMT Multi-Specimen Test System (Bruker Nano., USA) testing device. It was measured by pressing an indenter into the sample and recording the penetration depth and applied load simultaneously. Cyclic loading and unloading indentation tests were performed, increasing the maximum load at a constant rate of 10 N/min as the indenter penetrated the test specimen. Upon reaching the pre-set maximum value, the load was held at its maximum value for about 10 s before unloading the specimen at the same rate. Typically, cementitious materials show a large scatter of material properties compared to other homogeneous materials. Thus, several points were tested in the same characteristic region to ensure the accuracy and validity.

A typical micro-indentation load-displacement curve and a schematic representation of the micro-indentation test are shown in Fig. 2a and b. Where P_{max} denotes peak indentation load, h_t represents resultant impression depth, and h_{max} indicates peak load indentation depth. Unloading stiffness (S) and hardness (H) can be obtained using the expressions shown below:

$$H = \frac{P_{max}}{A} \tag{6}$$

$$S = \frac{\Delta P}{\Delta h} = \frac{2}{\sqrt{\pi}} E_r \sqrt{A} \tag{7}$$

where $\frac{1}{E_r} = \frac{(1-\upsilon^2)}{E} + \frac{(1-\upsilon_i^2)}{E_i}$, $E = (1-\upsilon^2)\left[\frac{1}{E_r} - \frac{1-\upsilon_i^2}{E_i}\right]^{-1}$, $E_i \& \upsilon_i$ are indenter tip parameters, A = Projected contact area at peak load, E_r = Reduced modulus, and $\upsilon \& E$ are sample's Poisson's ratio and Young's modulus, respectively (Table 2).

2.5.2. SEM-EDS imaging

Scanning Electron microscopy (SEM) imaging was performed on the samples with a Hitachi TM3030 SEM device to provide visual information on the microscopic characteristics of their surfaces. The SEM equipment was operated in high vacuum mode to ensure high-resolution imaging. During imaging, the SEM equipment was coupled with Energy-Dispersive X-ray Spectroscopy (EDS, Quantax70) to provide elemental identification of typical elements on the periodic table. The EDS spectrum provides information on the relative abundance of elements on the sample's surface. After SEM imaging and EDS analysis, the resulting images and spectra were interpreted to extract relevant information about the sample.

2.5.3. X-ray diffraction (XRD)

Before the analysis, the samples were first finely ground and homogenized. A BRUKER D8 FOCUS X X-ray diffractometer with high power (18 kW) and power rated 20–60 kV, 2–80 mA (stability: ±0.005%) was used in this study. It consists of three main elements: A sample holder, an X-ray tube, and an X-ray detector. The ground samples were placed on glass slides and placed on the holder. The test was then started by activating the cathode ray tube, and the intensity of the diffracted X-rays was continuously recorded.

3. Experimental results and discussion

3.1. Appearance and radial carbonation depth

The images in Fig. 3 provide visual evidence of the effects of high temperature (150 °C) and high partial pressure of CO_2-saturated brine (4 MPa) exposure on core samples of oil well cement blended with different additives. It can be seen in the first row that before exposure, the core samples have a dark grey color and a uniform texture, indicating a homogeneous cement matrix. After four weeks of exposure, the samples show a noticeable color change, turning from dark grey to yellowish-brown. The texture of the samples also

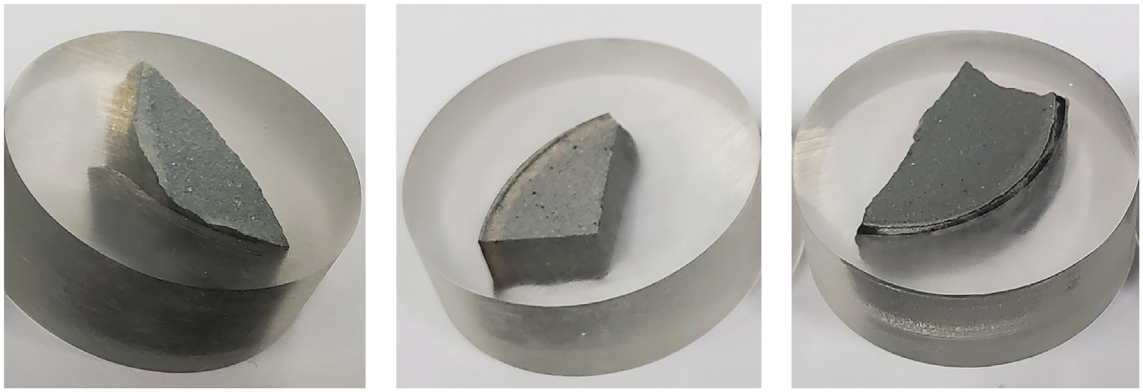

Fig. 1. Micro-indentation specimens in epoxy resin.

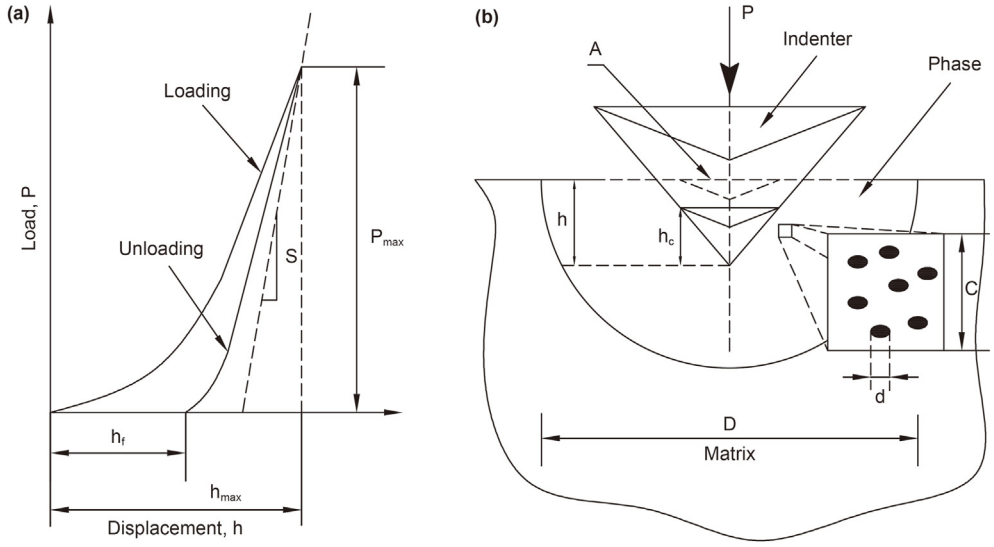

Fig. 2. (**a**) Typical micro-indentation load-depth curve. (**b**) schematic representation of the micro-indentation test.

Table 2
Micro-indentation test parameters.

Parameter	P_{max}, N	υ	E_i, GPa	υ_i
Value	30	0.26	1141	0.07

becomes more irregular. We applied a special indicator called phenolphthalein to examine the changes in the cement samples further. The indicator is colorless in solutions with a pH below 9 and turns pink in solutions with a pH above 9 (Mobin and Muthupriya, 2016; Bruckdorfer, 1986). When the indicator was sprayed on the freshly cut core surfaces of the reacted samples, it turned pink in the inner part of the samples, indicating that the inner part had a higher pH value.

In contrast, the outer part of the samples remained colorless, indicating a lower pH value, which is consistent with the decomposition of C–S–H into silica gel. Typically, the pH of cement pore fluid is about 13. However, in the process of CO_2 dissociation, the bicarbonate ions (HCO_3^-) are formed and react with cement hydration products, such as calcium silicate hydrate (C–S–H), leading to their decomposition into a mixture of calcite ($CaCO_3$) and amorphous silica gel (Duguid, 2009). Understanding the effects of CO_2 on cement properties is critical for the long-term performance of wellbore cement. The observed changes in the cement samples in this study suggest that exposure to high temperatures and CO_2 can lead to the deterioration of cement integrity, potentially compromising wellbore integrity and increasing the risk of leakage and environmental damage.

The carbonation depth of different cement formulations was measured at 14 and 28-day intervals to evaluate their susceptibility to CO_2 corrosion. The results showed that Mix 15, a silica fume blend, had a carbonation depth of about 3.24 mm after 14 days, which increased by about 47% (4.79 mm) on the 28th day. Similarly, Mix 16, a liquid silica blend, had a carbonation depth of about 1.67 mm on day 14, which increased by more than 48% by the 28th day. This increase indicates that the materials continued to undergo carbonation, suggesting that it was more susceptible to corrosion than the latex-blended cement. In contrast, the latex-blended cement showed the least radial carbonation depth (Fig. 4). The results suggest that adding different additives to oil well cement can significantly affect its resistance to CO_2-induced carbonation. The silica fume and liquid silica blends show lower carbonation resistance than the latex-blended cement, likely due to its ability to form a more dense matrix with superior CO_2 corrosion resistance properties.

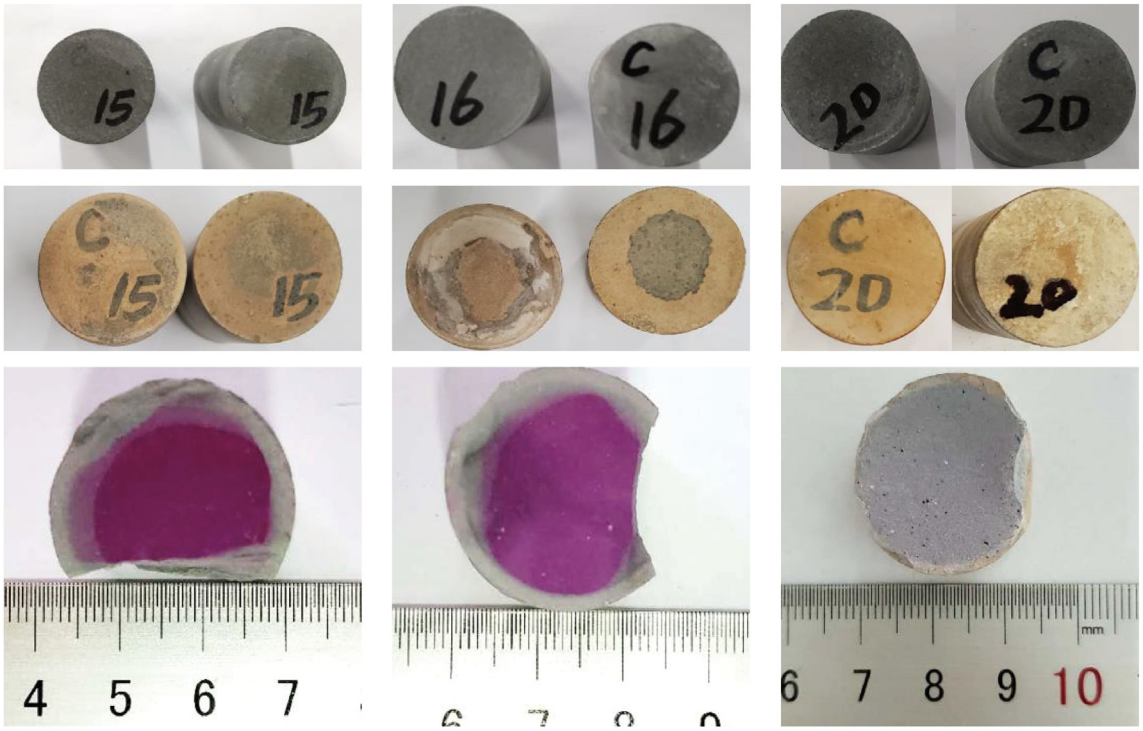

(a) Mix 15 **(b)** Mix 16 **(c)** Mix 20

Fig. 3. Samples appearance before and after corrosion (first row: Before corrosion; second row: after corrosion; third row: radial corrosion depth).

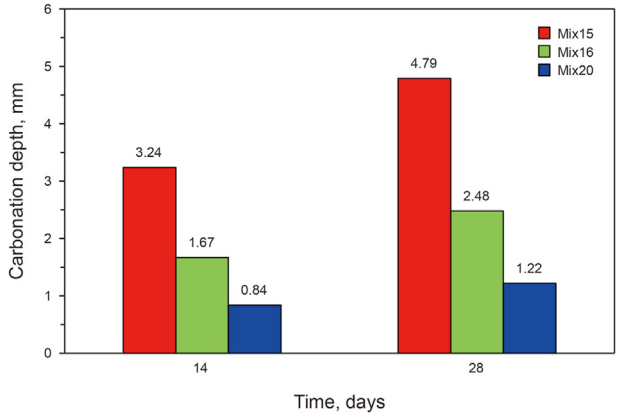

Fig. 4. Comparison of carbonation depth of different mixes after the reaction.

3.2. Effects of CO_2 exposure on compressive strength, porosity, and permeability

After 4-weeks of exposure to CO_2-saturated brine, all the samples showed a reduction in strength, as shown in Fig. 5a. The 10% liquid silica mix (Mix 16) experienced the highest decrease in compressive strength (about 26%), followed by the latex mix (Mix 20) and 10% silica fume mix (Mix 15), whose strengths dropped by 18% and 13%, respectively. The permeability of Mix 16 relatively decreased after exposure to CO_2-saturated brine, while that of Mix 15 and 20 increased. As shown in Fig. 5b, Mix 15 exhibited a 600% increase in permeability and an approximately 44% decrease in porosity (Fig. 5c). In comparison, Mix 20 experienced a considerably higher decrease in porosity (86%) and a relatively small increase in permeability (70%). Overall, Mix 16 exhibited superior qualities as demonstrated by changes in properties after exposure, as summarized in Fig. 5d. The change in permeability and porosity of different mixes after reaction can be attributed to various factors, such as the type and number of reactants, reaction conditions, and the resulting mineralogy and microstructure of the products. In the case of Mix 15 and Mix 20, the increase in permeability after the reaction could be due to the alteration of the existing mineralogy, which results in a more open and interconnected pore network. This can increase the size and number of pores, allowing for easier fluid flow and higher permeability. Additionally, the reaction may have caused some degree of compaction or compression of the sample, which could contribute to the observed increase in permeability.

On the other hand, the decrease in permeability observed in Mix 16 could be due to a reduction in pore size or the formation of more complex mineral structures that impede fluid flow. The small liquid silica particles surround the cement grains and fill the interstitial spaces between the larger cement particles. Subsequently, a dense crystal system of C–S–H is formed in these sites, reducing the percentage of interconnected pore voids. As for the porosity changes, Mix 15 and Mix 20 may have undergone a reduction in porosity due to the formation of new mineral phases or the alteration of existing phases. The reaction may have resulted in the filling or clogging of some of the pores, leading to decreased porosity. In contrast, Mix 16 may have experienced a slight increase in porosity due to the opening up of more pore space due to the reaction. It is important to note that the specific mechanism behind the observed changes in permeability and porosity will depend on the specific composition of the mixes and the conditions under which the reaction occurred.

In temperatures above 100 °C, pure Portland cement produces a poorly crystalline low permeability and high compressive strength C–S–H (II) phase. It is assumed that the corrosion C–S–H (II) phase is decomposed into α-C_2SH (α-dicalcium silicate hydrate) due to the

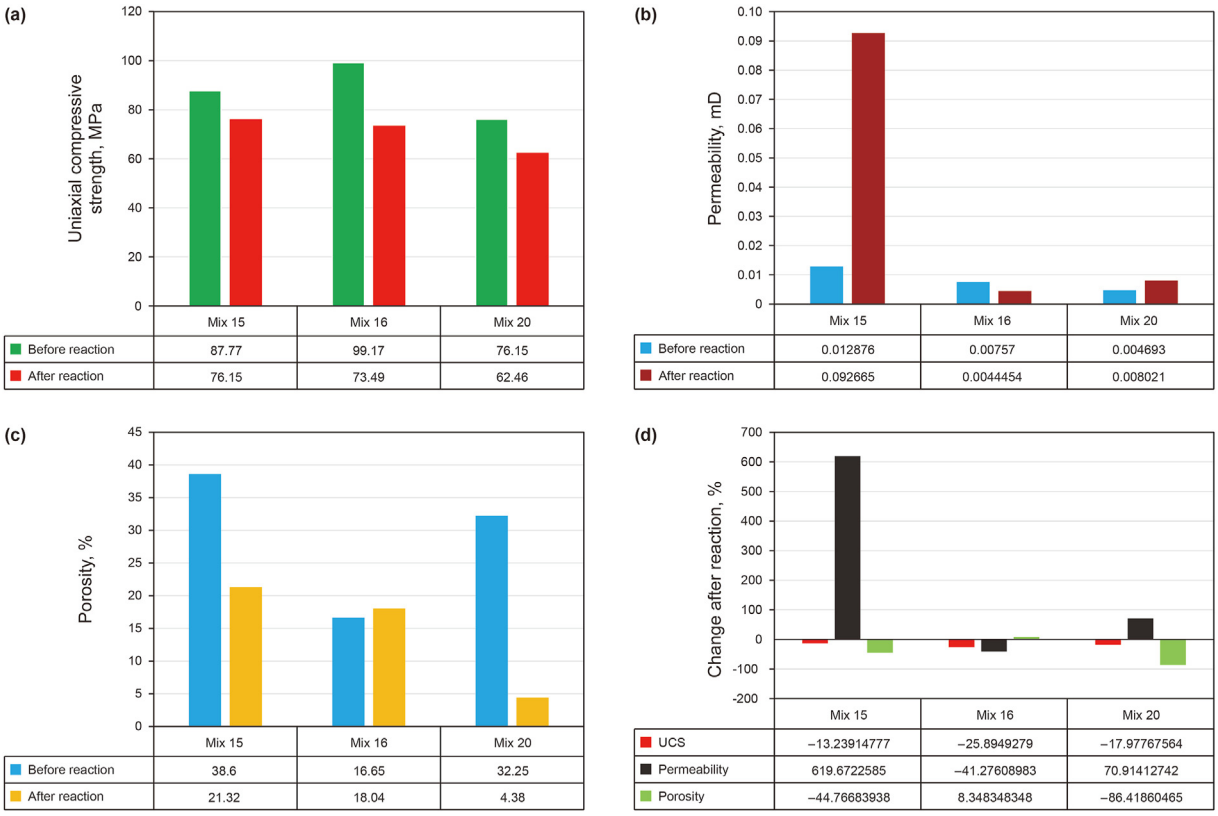

Fig. 5. Comparison of cement properties before and after CO_2 corrosion. (**a**): Uniaxial compressive strength (UCS). (**b**): Permeability. (**c**): porosity and change rate. (**d**): Percentage change in uniaxial compressive strength (UCS), permeability, and porosity.

absence of protective matters to prevent the deterioration of strength, resulting in poor performance compared with C–S–H after decomposition. However, adding admixtures such as silica and latex protects cement's mechanical and transport properties from deterioration. These admixtures are quite effective due to their small particle sizes, reactivity, and chemical composition.

When liquid silica is added to cement, it reacts with calcium hydroxide to produce a stable cementitious compound (secondary calcium silicate gel). The liquid silica chemical reaction is initiated when ionic species, including OH^-, Ca^{2+}, K^+, and Na^+, are released into the pore fluid of hydrated cement. In the presence of OH^- in the pore fluid, silica dissolves, producing silanol compounds (H_2SiO_4, H_3SiO_4, H_4SiO_4) which then readily react with Ca^{2+} and OH^- to produce secondary calcium silicate hydrate (CSH) as shown in Eq. (10) (Mueller and Dillenbeck, 1991).

$$H_4SiO_4(aq) + Ca^{2+}(aq) + 2OH^- \rightarrow n_1CaO \bullet SiO \bullet n_2H_2O(s) \quad (10)$$

This cement transformation enhances its strength simply because $Ca(OH)_2$ liberated during cement hydration is consumed to produce high-strength crystalline calcium silicate phases. Besides improving cement strength, silica admixtures reduce cement porosity, permeability, and its content of alkali compounds, all of which are critical properties in a CO_2-corrosive environment (Sadrmomtazi et al., 2018; Murtaza et al., 2013). Due to their small sizes, liquid and silica fume particles surround the cement grains and fill the interstitial spaces between the larger cement particles. Subsequently, a dense crystal system of C–S–H is formed in these sites, reducing the percentage of pore voids. In turn, the permeability of the set cement pastes decreases. Although silica fume is a good anti-corrosion admixture, it is believed that a high amount of silica can negatively affect cement properties (Vogt et al., 2021). This study demonstrates that liquid silica could be an effective alternative to silica fume.

Latex is an emulsified polymer material usually in the form of emulsion suspensions of very small spherical polymer particles (0.05–0.5 μm). The addition of a latex-based emulsion to cement-based materials can result in a significant improvement in compressive strength. This improvement is thought to be due to forming of a thin film of the latex-based emulsion around the cement hydration products. This film prevents direct contact between the hydration products and corrosive CO_2, which can impede the growth and propagation of microcracks. As a result, the cement exhibits a lower degree of deterioration over time, leading to better performance and longer service life. The film generated by the latex-based emulsion around the hydration products acts as a barrier between the cement hydration products and the surrounding environment (Jiao et al., 2016), including corrosive CO_2 and other factors that can cause microcracks to form and propagate. The film generated by the latex-based emulsion helps maintain the cement's structural integrity and reduces the risk of compressive strength decline by preventing the propagation of microcracks. In other words, the film helps to prevent further damage to the cement structure, which in turn helps maintain the material's compressive strength. It is important to note that the effectiveness of latex-based emulsions in improving cement-based materials' compressive strength depends on the type and proportion of the emulsion used. This mechanism explains why Mix 20 exhibited a lower compressive strength decrease. Nevertheless, further investigations are required to determine the proportions of these admixtures that can provide optimal results.

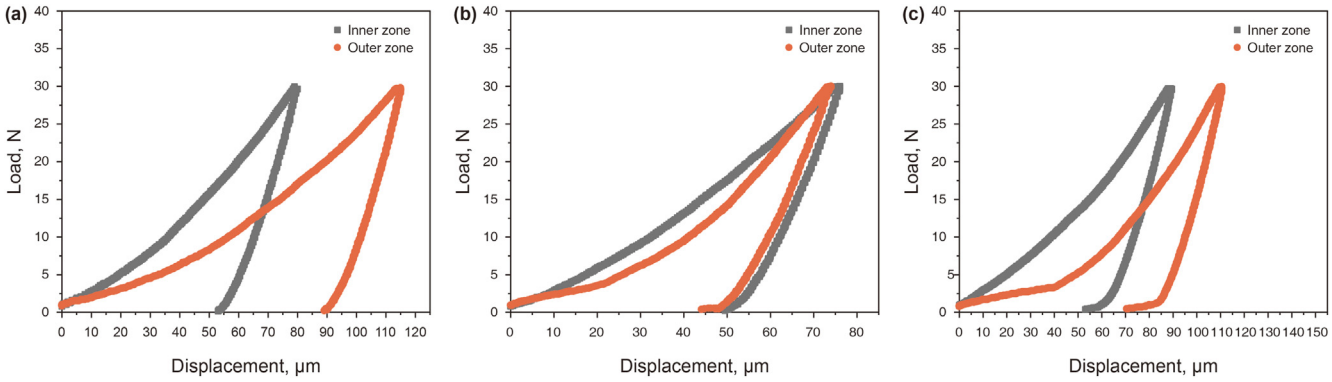

Fig. 6. Indentation load versus displacement curves for outer and inner zones. (**a**): Mix 15. (**b**) Mix 16. (**c**) Mix 20.

3.3. *Effects of CO_2 reaction on indentation depth and cement microstructural properties*

The nanoindentation test can effectively measure the mechanical properties of cementitious materials (Zhu and Bartos, 2000; Maragh et al., 2021). In addition, this test can provide a quantitative analysis of the micromechanical properties of various cement phases (Han et al., 2012b; Dejong and Ulm, 2007). As we have observed, exposure of cement to CO_2 results in the alteration of properties of cement hydration products. Major studies in this area mainly focus on altering mechanical and transport properties. However, nanoindentation analysis can provide us with a better understanding of micro-mechanical changes. In cement studies, this technology can be used to investigate the properties of cement hydration and carbonation products such as $Ca(OH)_2$, high-density hydrated calcium silicate (HD-CSH), and low-density calcium silicate hydrate (LD-CSH) (Li et al., 2021; Zhang et al., 2019). The mechanical properties of C–S–H are said to decrease significantly after leaching and contaminant decalcification. Therefore, as chemical degradation progresses, different layers with different phase compositions will have varying micromechanical properties.

Fig. 6 shows the load against displacement curves of the indentation test of the three mixes. Mix 16 (Fig. 6b) outer layer shows a maximum penetration depth at a peak load of about 70 μm, while Mix 15 (Fig. 6a) and Mix 20 (Fig. 6c) are 115 μm and 110 μm, respectively, indicating that Mix 15 and 20 outer zones become relatively soft after corrosion. It is also evident that the rate of change of the microstructure of Mix 16 after exposure to CO_2-saturated brine is relatively slow.

The mechanical properties of sample cross-section can vary significantly at small scales, making it difficult to obtain accurate and reliable measurements from a single point on the surface of a material. This heterogeneity was accounted for by performing micro-indentation measurements at multiple points on a sample surface, and the average value and error bars were calculated. Using Oliver and Pharr's method (Oliver and Pharr, 1992), the average elastic modulus and hardness are calculated from the load versus displacement curves (Fig. 7a and b). The result shows that different cement phases have different micromechanical properties. In addition, compared with the carbonation product ($CaCO_3$), the elastic modulus and hardness of the hydration products ($Ca(OH)_2$ and CSH) are significantly different. The elastic modulus for the outer zone of Mix 15, Mix 16, and Mix 20 are 24.99 GPa, 29.73 GPa, and 18.03 GPa, respectively. It can also be seen that the outer zone of Mix 16 possesses a high hardness of about 1.26 GPa compared to 0.99 and 0.58 GPa for Mix 15 and Mix 20, respectively. Generally, the outer and inner zones of Mix 16 exhibited high hardness and elastic modulus. The Mix 20 exhibited relatively small hardness and elastic modulus. As such, most of the indenter displacement in Mix 20 is accommodated plastically (Fig. 6c); thus, its percentage recovery on unloading is small compared to Mix 16. The elastic modulus results obtained using the micro-indentation test are similar to those obtained by the conventional triaxial test. Upon exposure to a corrosive environment, the degree of change in cement microstructural properties varies with zones. Zhang et al. (2013) showed that the rim region of the 35-vol% pozzolan samples exhibited a higher microhardness than that of the core region for the same sample. As we have demonstrated, significant deterioration occurs in zones in direct contact with corrosive fluids. However, It is important to note that the wetting behavior of CO_2 droplets can change the strength of solid-liquid attraction, as demonstrated by Wu et al. (2020), and merit consideration in future research.

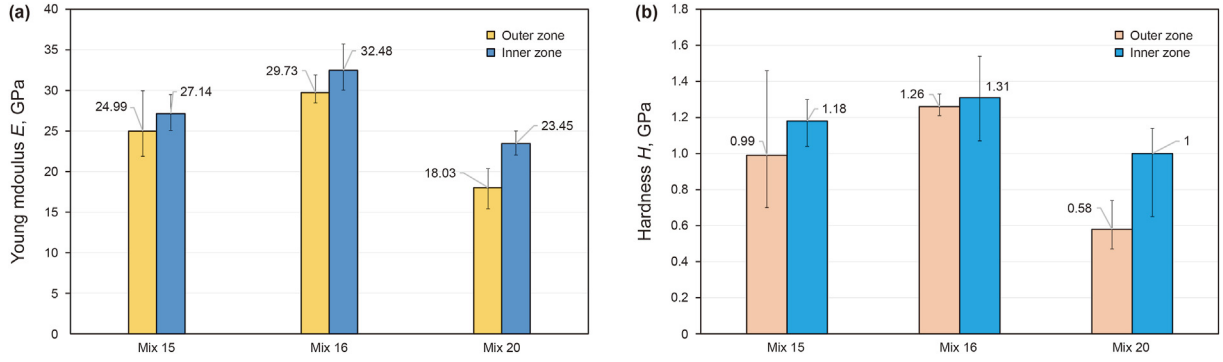

Fig. 7. Comparison of micro-indentation results of cement paste's hydration and carbonization corrosion products. (**a**): Young modulus of the outer and inner zone. (**b**): Hardness of outer and inner zone.

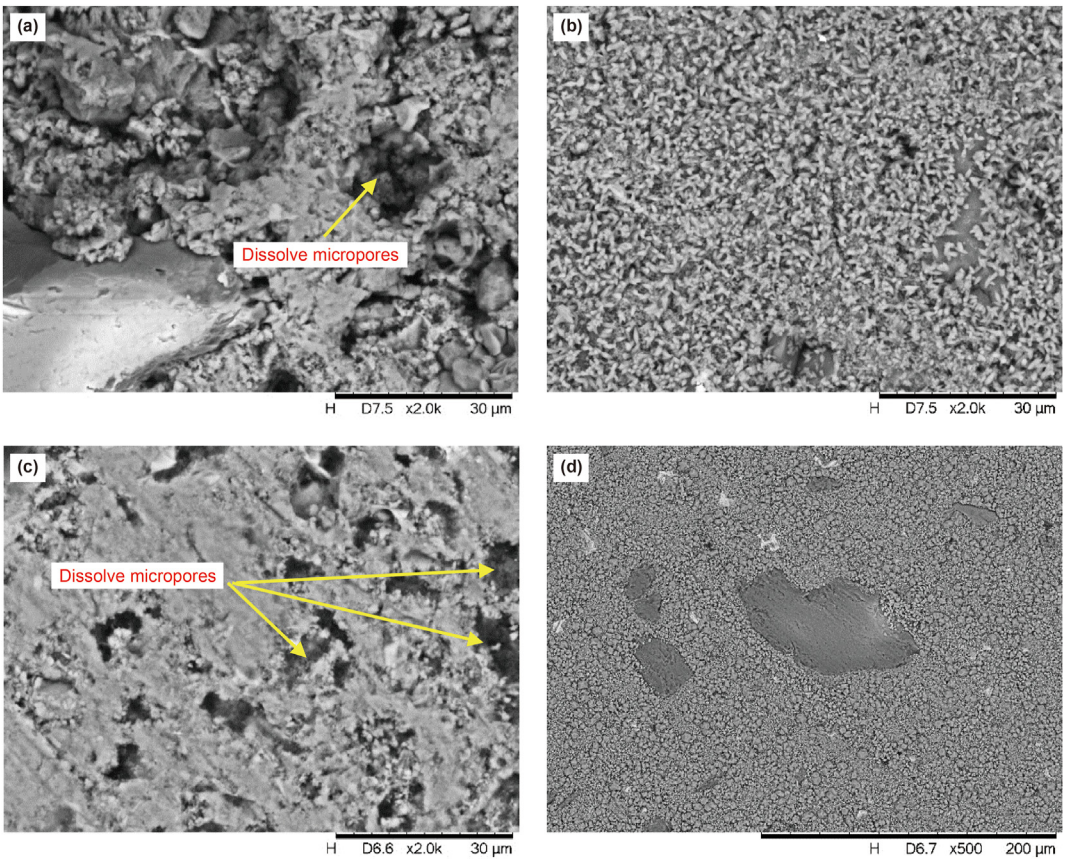

Fig. 8. Surface micro-morphology images of inner and outer layers. (**a**): the corroded outer layer of Mix16. (**b**): dense inner layer of Mix 16. (**c**): the corroded outer layer of Mix 20. (**d**): dense inner layer of Mix 20.

3.4. SEM and XRD analysis

SEM and XRD analysis of the specimens confirms that the exposure of cement samples to CO_2-saturated brine altered their microstructural properties. As shown in SEM micrograph images in Fig. 8, the specimens' outer zones became more porous after exposure. However, the inner zones remained relatively dense, with fewer voids and pore spaces. These results conform with indentation test data and support porosity and permeability changes observed after exposure. Essentially, after extended exposure to a corrosive environment, the dissolution of cement hydration products and precipitation of carbonation products occurs within the cement matrix. These processes alter the internal microstructure leading to a loose and porous matrix with a significant change in its average elastic modulus and hardness noted in the outer and inner zones.

XRD tests are useful for analyzing the crystalline phase of the cement samples. Miao et al. (2020) used X-ray computed microtomography to characterize the microstructure alteration of wellbore cement under geologic carbon storage, proposing a framework

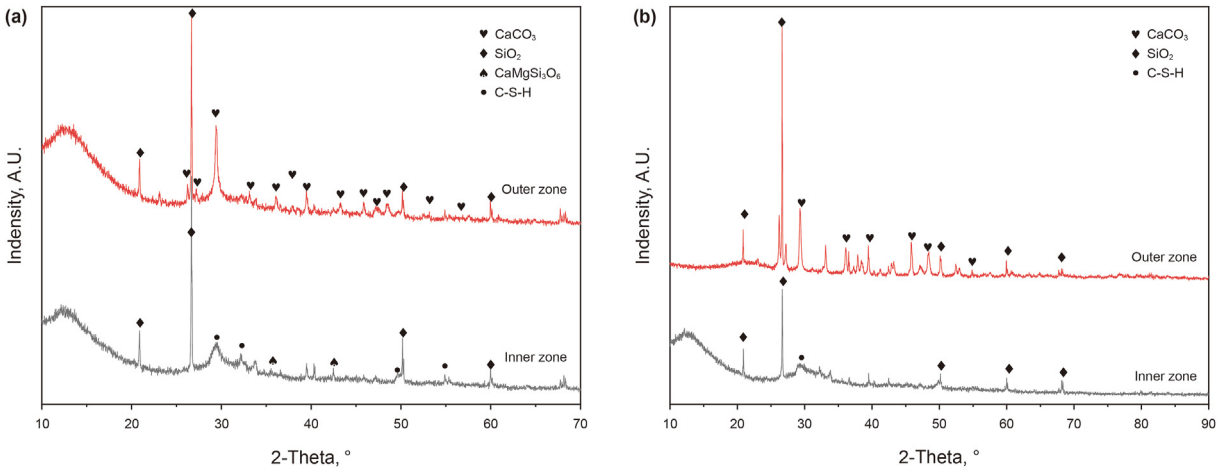

Fig. 9. XRD pattern of cement inner and outer layers after CO_2 environmental corrosion. (**a**): Mix 16 (with 10% liquid silica cement). (**b**): Mix 20 (with 16% latex cement outer layer).

for fast CT image registration and carbonate shell morphology quantification (Miao et al., 2020). Each phase has a unique characteristic peak intensity proportional to its concentration. When ordinary Portland cement is mixed with admixtures, the concentration of its hydration products changes significantly. Similarly, when exposed to CO_2 environments, the hydration products are transformed into carbonation products, and their concentration decreases. The XRD of the outer zones of both Mix16 and Mix 20 shows a high content of $CaCO_3$ and no traces of CSH (Fig. 9). The absence of calcium hydroxide (CH) and reduction of the other hydration peaks affirm the corrosion of the outer layers and the alteration of cement microstructure when immersed in CO_2 saturated brine. Generally, the decomposition of cement hydration products, particularly the C–S–H phase, and the resultant increase of microporosity largely contribute to the loss of stiffness in the outer layers. As expected, the inner zones have large quantities of calcium silicate hydrate (C–S–H) and no carbonation products, which explains why these zones have superior mechanical properties.

4. Conclusions

In this study, a series of experiments were performed to determine the effects of chemo-mechanical degradation on the properties of different oil well cement formulations. The influences of CO_2 on mechanical, transport, and microstructural characteristics of well oil cement modified with Silica fume, liquid silica, and latex were studied. The findings could be useful in designing cement-based materials that are more corrosion-resistant and can maintain their performance over time. The following conclusions can be drawn.

(1) Strength retrogression control admixtures refine the cement pore structure by surrounding its grains and occupying interstices between cement hydration products, thus densifying its matrix.
(2) Silica fume and liquid silica produce additional C–S–H by pozzolanic reaction reducing the C/S ratio. However, the C–S–H produced by silica fume are thermodynamically unstable and thus transform to low-strength C–S–H phases. Liquid silica is an effective alternative to silica fume in sour gas HPHT wells. Moreover, managing and eliminating the health and environmental risk associated with dry blending is easier.
(3) The findings suggest that the micromechanical properties of different cement phases vary, with the elastic modulus and hardness of the hydration products ($Ca(OH)_2$ and C–S–H) being significantly different from those of the carbonation product ($CaCO_3$). The outer and inner zones of cement Mix 16 exhibit high hardness and elastic modulus. Mix 20 displays relatively small hardness and elastic modulus, indicating that most of the indenter displacement in Mix 20 is accommodated plastically.
(4) This analysis demonstrates that the micro-indentation test can provide a useful method for evaluating the mechanical-chemical degradation of cement.

Declaration of competing interest

The authors declare that they have no known competing financial interests or personal relationships that could have appeared to influence the work reported in this paper.

Acknowledgments

This work was funded by National Natural Science Foundation Project (Grant No.52274015) & Opening Project Fund of Materials Service Safety Assessment Facilities (MSAF-2021-102).

References

Bruckdorfer, R.A., 1986. Carbon dioxide corrosion in oilwell cements. SPE rocky mountain regional meeting. OnePetro. https://doi.org/10.2118/15176-MS.
Constantinides, G., Ulm, F.J., Van Vliet, K., 2003. On the use of nanoindentation for cementitious materials. Mater. Struct. 36, 191–196. https://doi.org/10.1007/BF02479557.
Chang, C.F., Chen, J.W., 2006. The experimental investigation of concrete carbonation depth. Cement Concr. Res. 36 (9), 1760–1767. https://doi.org/10.1016/j.cemconres.2004.07.025.
Carroll, S., Carey, J.W., Dzombak, D., Huerta, N.J., Li, L., Richard, T., Um, W., Walsh, S.D.C., Zhang, L., 2016. Role of chemistry, mechanics, and transport on well integrity in CO_2 storage environments. Int. J. Greenh. Gas Control. 49, 149–160. https://doi.org/10.1016/j.ijggc.2016.01.010.
Chavez Panduro, E.A., Cordonnier, B., Gawel, K., Børve, I., Iyer, J., Carroll, S.A., et al., 2020. Real time 3D observations of Portland cement carbonation at CO_2 storage conditions. Environ. Sci. Technol. 54 (13), 8323–8332. https://doi.org/10.1021/acs.est.0c00578.
Carpenter, C., 2022. Challenges overcome in drilling and testing a deep, deviated HP/HT offshore gas well. J. Petrol. Technol. 74 (3), 81–83. https://doi.org/10.2118/0322-0081-JPT.
DeJong, M.J., Ulm, F.J., 2007. The nanogranular behavior of CSH at elevated temperatures (up to 700 °C). Cement Concr. Res. 37 (1), 1–12. https://doi.org/10.1016/j.cemconres.2006.09.006.
Duguid, A., 2009. An estimate of the time to degrade the cement sheath in a well exposed to carbonated brine. Energy Proc. 1 (1), 3181–3188. https://doi.org/10.1016/j.egypro.2009.02.101.
Duguid, A., Scherer, G.W., 2010. Degradation of oilwell cement due to exposure to carbonated brine. Int. J. Greenh. Gas Control 4 (3), 546–560. https://doi.org/10.1016/j.ijggc.2009.11.001.
Gherardi, F., Audigane, P., Gaucher, E.C., 2012. Predicting long-term geochemical alteration of wellbore cement in a generic geological CO_2 confinement site: tackling a difficult reactive transport modeling challenge. J. Hydrol. 420, 340–359. https://doi.org/10.1016/j.jhydrol.2011.12.026.
Gu, T., Guo, X., Li, Z., Cheng, X., Fan, X., Korayem, A., Duan, W.H., 2017. Coupled effect of CO_2 attack and tensile stress on well cement under CO_2 storage conditions. Construct. Build. Mater. 130, 92–102. https://doi.org/10.1016/j.conbuildmat.2016.10.117.
Huet, B.M., Prevost, J.H., Scherer, G.W., 2010. Quantitative reactive transport modeling of Portland cement in CO_2-saturated water. Int. J. Greenh. Gas Control. 4 (3), 561–574. https://doi.org/10.1016/j.ijggc.2009.11.003.
Han, J., Pan, G., Sun, W., 2012a. Elastic modulus change investigation of cement paste before and after carbonation using nanoindentation technique. Procedia Eng. 27, 341–347. https://doi.org/10.1016/j.proeng.2011.12.461.
Han, J., Pan, G., Sun, W., Wang, C., Cui, D., 2012b. Application of nanoindentation to investigate chemo-mechanical properties change of cement paste in the carbonation reaction. Sci. China Technol. Sci. 55, 616–622. https://doi.org/10.1007/s11431-011-4571-1.
Jiao, L.B., Chen, D.J., Feng, D.Y., Wang, X.M., Zhang, J., 2016. Potential for significantly improving performances of oil-well cement by soap-free emulsions. Mater. Struct. 49, 279–288. https://doi.org/10.1617/s11527-014-0495-0.
Kutchko, B.G., Strazisar, B.R., Dzombak, D.A., Lowry, G.V., Thaulow, N., 2007. Degradation of well cement by CO2 under geologic sequestration conditions. Environ. Sci. Technol. 41 (13), 4787–4792. https://doi.org/10.1021/es062828c.
Kutchko, B.G., Strazisar, B.R., Huerta, N., Lowry, G.V., Dzombak, D.A., Thaulow, N., 2009. CO_2 reaction with hydrated class H well cement under geologic sequestration conditions: effects of flyash admixtures. Environ. Sci. Technol. 43 (10), 3947–3952. https://doi.org/10.1021/es803007e.
Kiran, R., Teodoriu, C., Dadmohammadi, Y., Nygaard, R., Wood, D., Mokhtari, M., Salehi, S., 2017. Identification and evaluation of well integrity and causes of failure of well integrity barriers (A review). J. Nat. Gas Sci. Eng. 45, 511–526. https://doi.org/10.1016/j.jngse.2017.05.009.
Li, Y., She, C., Liu, N., Zhang, H., Zhang, L., Zhu, D., 2016. Completion difficulties of HTHP and high-flowrate sour gas wells in the Longwangmiao Fm gas reservoir, Sichuan Basin, and corresponding countermeasures. Nat. Gas. Ind. B 3 (3), 269–273. https://doi.org/10.1016/j.ngib.2016.05.012.
Li, L.I., Li, Z., Cao, M., Tang, Y.I., Zhang, Z.H.E., 2021. Nanoindentation and porosity fractal dimension of calcium carbonate whisker reinforced cement paste after elevated temperatures (up to 900 °C). Fractals 29 (2), 2140001. https://doi.org/10.1142/S0218348X21400016.
Mueller, D.T., Dillenbeck, R.L., 1991. The versatility of silica fume as an oilwell cement admixture. SPE Production Operations Symposium. OnePetro. https://doi.org/10.2118/21688-MS.
Murtaza, M., Rahman, M.K., Al-Majed, A.A., Samad, A., 2013. Mechanical, rheological and microstructural properties of saudi type g cement slurry with silica flour used in saudi oil field under hthp conditions. In: SPE Saudi Arabia Section

Technical Symposium and Exhibition. OnePetro. https://doi.org/10.2118/168101-MS.
Mobin, T.R., Muthupriya, P., 2016. Determination of concrete carbonation depth by experimental investigation. Int. J. Eng. Sci. Invent. Res. Dev. 2 (8), 534–541.
Miao, X., Zhang, L., Wang, Y., Wang, L., Fu, X., Gan, M., Li, X., 2020. Characterisation of wellbore cement microstructure alteration under geologic carbon storage using X-ray computed micro-tomography: a framework for fast CT image registration and carbonate shell morphology quantification. Cement Concr. Compos. 108, 103524. https://doi.org/10.1016/j.cemconcomp.2020.103524.
Maragh, J.M., Palkovic, S.D., Shukla, A., Büyüköztürk, O., Masic, A., 2021. SEM-EDS and microindentation-driven large-area high-resolution chemo-mechanical mapping and computational homogenization of cementitious materials. Mater. Today Commun. 28, 102698. https://doi.org/10.1016/j.mtcomm.2021.102698.
Oliver, W.C., Pharr, G.M., 1992. An improved technique for determining hardness and elastic modulus using load and displacement sensing indentation experiments. J. Mater. Res. 7 (6), 1564–1583. https://doi.org/10.1557/JMR.1992.1564.
Parrott, L.J., 1987. A Review of Carbonation in Reinforced Concrete. Cement and Concrete Association, London.
Phi, T., Elgaddafi, R., Al Ramadan, M., Ahmed, R., Teodoriu, C., 2019. Well integrity issues: extreme high-pressure high-temperature wells and geothermal wells a review. SPE Thermal Well Integrity and Design Symposium. OnePetro. https://doi.org/10.2118/198687-MS.
Shadravan, A., Amani, M., 2012. HPHT 101-what every engineer or geoscientist should know about high pressure high temperature wells. SPE Kuwait International Petroleum Conference and Exhibition. OnePetro. https://doi.org/10.2118/163376-MS.
Sadrmomtazi, A., Tahmouresi, B., Kohani Khoshkbijari, R., 2018. Effect of fly ash and silica fume on transition zone, pore structure and permeability of concrete. Mag. Concr. Res. 70 (10), 519–532. https://doi.org/10.1680/jmacr.16.00537.
Todorovic, J., Opedal, N.V., Werner, B., Angelique Clausen, J., Jæger Sweetman Kvassnes, A., 2020. Effect of long-term aging in carbonated brine on mechanical properties of a novel cement system with an expandable agent. SPE Norway subsurface conference. OnePetro. https://doi.org/10.2118/200753-MS.
Vogt, O., Ukrainczyk, N., Koenders, E., 2021. Effect of silica fume on metakaolin geopolymers' sulfuric acid resistance. Materials 14 (18), 5396. https://doi.org/10.3390/ma14185396.
Woirgard, J., Tromas, C., Girard, J.C., Audurier, V., 1998. Study of the mechanical properties of ceramic materials by the nanoindentation technique. J. Eur. Ceram. Soc. 18 (15), 2297–2305. https://doi.org/10.1016/S0955-2219(98)00083-1.
Wei, P., Juan, D., Tongyi, Z., Zhiguo, Q., Gang, L., 2015. Well testing technique for HPHT sour gas wells in China. Offshore technology conference. OnePetro. https://doi.org/10.4043/25681-MS.
Wu, J., Snustad, I., Ervik, Å., Brunsvold, A., He, J., Zhang, Z., 2020. CO_2 wetting on pillar-nanostructured substrates. Nanotechnology 31 (24), 245403. https://doi.org/10.1088/1361-6528/ab7c49.
Zhu, W., Bartos, P.J., 2000. Application of depth-sensing microindentation testing to study of interfacial transition zone in reinforced concrete. Cement Concr. Res. 30 (8), 1299–1304. https://doi.org/10.1016/S0008-8846(00)00322-7.
Zhang, L., Dzombak, D.A., Nakles, D.V., Hawthorne, S.B., Miller, D.J., Kutchko, B.G., Lopano, C.L., Strazisar, B.R., 2013. Characterization of pozzolan-amended wellbore cement exposed to CO_2 and H_2S gas mixtures under geologic carbon storage conditions. Int. J. Greenh. Gas Control. 19, 358–368. https://doi.org/10.1016/j.ijggc.2013.09.004.
Zhang, H., Šavija, B., Luković, M., Schlangen, E., 2019. Experimentally informed micromechanical modelling of cement paste: an approach coupling X-ray computed tomography and statistical nanoindentation. Compos. B Eng. 157, 109–122. https://doi.org/10.1016/j.compositesb.2018.08.102.
Zhang, H., Romero Rodriguez, C., Dong, H., Gan, Y., Schlangen, E., Šavija, B., 2020a. Elucidating the effect of accelerated carbonation on porosity and mechanical properties of hydrated portland cement paste using X-ray tomography and advanced micromechanical testing. Micromachines 11 (5), 471. https://doi.org/10.3390/mi11050471.
Zhang, H., Xu, Y., Gan, Y., Chang, Z., Schlangen, E., Šavija, B., 2020b. Microstructure informed micromechanical modelling of hydrated cement paste: techniques and challenges. Construct. Build. Mater. 251, 118983. https://doi.org/10.1016/j.conbuildmat.2020.118983.